

A Unique Multi-Messenger Signal of QCD Axion Dark Matter

Thomas D. P. Edwards,^{*} Marco Chianese,[†] Bradley J. Kavanagh,[‡] Samaya M. Nissanke,[§] and Christoph Weniger[¶]
*Gravitation Astroparticle Physics Amsterdam (GRAPPA),
 Institute for Theoretical Physics Amsterdam and Delta Institute for Theoretical Physics,
 University of Amsterdam, Science Park 904, 1090 GL Amsterdam, The Netherlands*

(Dated: October 11, 2024)

We propose a multi-messenger probe of the natural parameter space of QCD axion dark matter based on observations of black hole-neutron star binary inspirals. It is suggested that a dense dark matter spike may grow around intermediate mass black holes ($10^3 - 10^5 M_\odot$). The presence of such a spike produces two unique effects: a distinct phase shift in the gravitational wave strain during the inspiral and an enhancement of the radio emission due to the resonant axion-photon conversion occurring in the neutron star magnetosphere throughout the inspiral and merger. Remarkably, the observation of the gravitational wave signal can be used to infer the dark matter density and, consequently, to predict the radio emission. We study the projected sensitivity to the axion-photon coupling in the light of the LISA interferometer and next-generation radio telescopes such as the Square Kilometre Array. Given a sufficiently nearby detection, such observations will explore the QCD axion in the mass range 10^{-7} eV to 10^{-5} eV.

Introduction — The particle nature of Dark Matter (DM) remains a mystery to physicists [1, 2] despite numerous experimental efforts to observe its effects in lab-based experiments and indirectly through astrophysical observations [3–6]. Another fundamental indication of New Physics comes from the strong charge parity (CP) problem of quantum chromodynamics (QCD) [7]. CP violation in the QCD sector could generically be large but instead appears to be fine-tuned below observable limits. The most popular solution to this issue is the Peccei-Quinn mechanism, which predicts the existence of the *axion* [8–11]. Axion-like particles are also predicted in several extensions of the Standard Model and they are expected to appear in string theory [12]. However, only in the case of the QCD axion is there a tight relation between its mass and its couplings with ordinary matter [13–17].

These two fundamental issues can be addressed simultaneously by treating the QCD axion as a DM candidate [18]. The DM axion may be produced with the correct relic abundance through the misalignment mechanism [19] (though see e.g. Refs. [20, 21] for alternatives). So far, only a small part of the QCD axion parameter space has been explored due to its weak interaction with matter [22, 23]. However, new experimental techniques to search for axions have been recently proposed [24–35] (see Ref. [36] for a comprehensive review). Furthermore, it has recently been noted that the Primakov effect can efficiently convert axions to photons in the magnetic fields of Neutron Stars (NSs). These photons are potentially observable with current and future radio telescopes, provided the axion-photon coupling strength is large enough

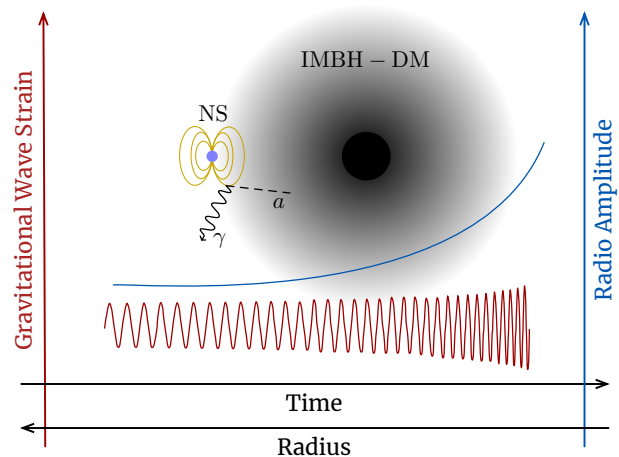


FIG. 1. **Illustration of the IMBH-DM-NS system.** The presence of an axion DM halo around the intermediate mass black hole (IMBH) produces a phase shift in the strain of the GW signal and radio emission due to its conversion into photons in the neutron star (NS) magnetosphere. a and γ represent an axion and radio photon respectively.

[37–39].

The recent discovery of Gravitational Waves (GWs) has provided a new observational portal into extreme astrophysical environments [40]. The detection of the binary NS merger GW170817 and follow up electromagnetic counterparts further revolutionised astrophysics and truly defined the beginning of the multi-messenger era [41, 42]. Distortions to the GWs from binary black holes, caused by finite size effects of superradiant clouds, have recently been shown to also provide a new probe of beyond the standard model (BSM) physics [43, 44]. References [45, 46] have shown that the presence of a DM mini-spike around an intermediate mass black hole (IMBH) can dramatically affect the GW waveform through dynamical friction, providing yet another direct

* t.d.p.edwards@uva.nl

† m.chianese@uva.nl

‡ b.j.kavanagh@uva.nl

§ s.m.nissanke@uva.nl

¶ c.weniger@uva.nl

probe of BSM physics. DM environmental effects on GW signals were studied more generally in Refs. [47, 48].

In this *Letter*, we explore the possibility of probing the natural range of QCD axion DM parameters with multi-messenger astronomy. To make this possible we utilise the combined signal of GWs and radio emission from a NS inspiraling towards an IMBH surrounded by a dense spike of axion DM. This idea is sketched in Fig. 1. We show that by measuring the spike profile from the GW signal using LISA [49] (the space-based GW observatory planned for launch in the 2030s) we can predict the gradual evolution of the radio signal during the inspiral phase. Most importantly, the increased density due to the mini-spike amplifies the signal dramatically, allowing one to probe the axion coupling to photons for the most commonly used QCD axion models [13–16]. We start by describing the astrophysical system and possible formation mechanisms. Next we discuss the GW signal and radio emission followed by the instrumental sensitivities of LISA and the Square Kilometre Array (SKA) [50], for 5 years and 100 hours of observation time respectively. Finally, we present projected constraints on the DM density profile (Fig. 2) and sensitivities to the axion couplings (Fig. 3) before discussing caveats, including the likelihood of observing such an astrophysical setup.

Astrophysical System — IMBHs are a class of BHs with masses $M_{\text{BH}} = 10^2 - 10^5 M_{\odot}$. Thought to reside in the centres of smaller spiral galaxies, as well as in dense stellar environments such as globular clusters [51], a growing number of observations point toward the existence of IMBHs in nature [52–55]. In addition, there are multiple plausible formation mechanisms, such as runaway growth through the mergers of stellar mass objects [56–58]; by the direct collapse of gas clouds at high redshift [59, 60]; or primordial formation through the collapse of large density perturbations before Big Bang Nucleosynthesis [61–63].

These IMBHs may exist in DM halos [64–67]. It has been shown that for collisionless DM particles, a BH residing in the centre of the halo will go through adiabatic growth [68]. The DM is then expected to form a dense spike whose density profile $\rho_{\text{DM}}(r)$ is a power law with index α given by [68–71]:

$$\rho_{\text{DM}}(r) = \begin{cases} \rho_{\text{sp}} \left(\frac{r_{\text{sp}}}{r}\right)^\alpha, & r_{\text{ISCO}} < r \leq r_{\text{sp}} \\ \frac{\rho_s}{(r/r_s)(1+r/r_s)^2}, & r > r_{\text{sp}}. \end{cases} \quad (1)$$

The NFW parameters ρ_s and r_s [72] are related to the cosmological history and mass of the halo, for which we follow the same prescription as in Ref. [46], assuming a formation redshift of $z_f = 20$ and a total halo mass of $10^6 M_{\odot}$. The radius of the BH's inner-most stable circular orbit (ISCO) is denoted as r_{ISCO} . To solve for the spike parameters we use the empirical definition $r_{\text{sp}} \sim 0.2 r_h$ and the gravitational influence of the central IMBH given by $M(< r_h) = 4\pi \int_{r_{\text{ISCO}}}^{r_h} \rho_{\text{DM}} r^2 dr = 2M_{\text{BH}}$ [46]. The spike profile can vary depending on the initial DM profile. For an initially NFW-like profile, $\alpha = 7/3$,

which we take as our baseline scenario. For the spike to be preserved, the BH must not have gone through any mergers in its recent past, nor have a dense and highly energetic accretion disk [73, 74]. Globular cluster IMBHs therefore represent the most likely location for this system [75, 76].

In addition to the IMBH with surrounding DM halo, we consider an inspiraling NS (on a circular orbit, for concreteness). NSs can have extremely high magnetic fields ($10^9 - 10^{15}$ G), allowing for efficient axion-photon conversion close to the NS surface. NSs are readily formed in globular clusters and are therefore plausible candidates for mergers with IMBHs. We refer to the total system as IMBH-DM-NS.

Reference [64] argues that there are many IMBHs within our own Galactic halo. For an IMBH-DM-NS system to form, the IMBH must capture a NS. This process is very uncertain, relying on tracing formation models from the early Universe to today [75, 77]. Reference [75] suggests that the detection rate density in LISA will be approximately $\mathcal{R} \sim 3 - 10 \text{ Gpc}^{-3} \text{ yr}^{-1}$. We therefore consider two scenarios, one in which the IMBH-DM-NS system is close, at 0.01 Gpc, and one in which the system is further away, at 1 Gpc. The former is an optimistic scenario in terms of the strength of the radio signal, whereas many more of these farther systems are likely to be observed over a ten year observing period¹. Importantly, these events are dominated by IMBHs with masses $10^3 - 10^4 M_{\odot}$. For concreteness we consider an IMBH of $10^4 M_{\odot}$ since the additional gravitational potential of the BH preserves the structure of the spike for longer times [78]. We will discuss this assumption further below.

Finally, we must make some assumptions for the parameters of the inspiralling NS. NS populations in globular clusters are thought to be much older than those of normal pulsars found in galactic disks. These populations are also uncertain, though it is thought that most NSs are formed from electron-capture supernova processes due to their minimal kick velocities [37, 76]. We therefore take the magnetic field strength and spin period as 10^{12} G and 10 s respectively [38, 76]. Note that similar NSs have been found in observed globular clusters [79–83]. Moreover, we also assume $M_{\text{NS}} = 1.4 M_{\odot}$ and $r_{\text{NS}} = 10$ km as benchmark values for the mass and the radius of the NS.

Multi-Messenger Signals — There are two messengers for the system, a distinct phase shift in the gravitational wave strain and radio emission from axion-photon conversion in the plasma of the NS. Both signals increase as the NS approaches the IMBH, where a higher DM density is expected. The GW signal can be used to infer the DM density around the IMBH, so making a prediction for the axion radio emission.

¹ We note that 1 Gpc corresponds to $z \approx 0.25$ and a signal-to-noise ratio of ~ 1 in LISA.

Both signatures rely on the assumption that the DM can be treated as a particle, rather than a wave, therefore limiting us to axion masses $m_a > 10^{-7}$ eV. The corresponding Compton wavelength is 0.01 km, significantly smaller than the size of the NS. We therefore assume the spike acts as cold dark matter. We also require that the axion-photon conversion occurs exterior to the NS, setting an upper limit of $m_a < 1.4 \times 10^{-5}$ eV. We now discuss each signal in turn.

The dominant effect to cause a deviation from the vacuum inspiral signal is the gravitational interaction between the halo of DM particles and the NS passing through it, known as dynamical friction (DF) [84–86]. Dynamical friction exerts a drag force on the NS:

$$f_{\text{DF}} = 4\pi G_N^2 M_{\text{NS}}^2 \frac{\rho_{\text{DM}}(r)}{v_{\text{NS}}^2(r)} \ln \Lambda, \quad (2)$$

where G_N is the gravitational constant, v_{NS} is the velocity of the NS, and we take $\ln \Lambda \sim 3$ for the Coulomb logarithm. This force causes a loss of orbital energy from the NS, changing the accumulated phase of the GW signal and eventually reducing the inspiral time before merger with respect to the vacuum waveform. We see from Eq. (2) that this force grows as the NS inspirals², although so too does the radiation reaction force due to the emission of GWs.

In the Newtonian regime, the frequency-domain waveform of the IMBH-DM-NS system is computed by solving the energy balance equations, taking into account the effect of both DF and GW emission on the orbital energy of the system [46]. The resulting phase difference with respect to the vacuum inspiral signal depends both on the chirp mass $\mathcal{M}_c \simeq M_{\text{NS}}^{3/5} M_{\text{BH}}^{2/5}$ and on the individual masses M_{BH} and M_{NS} ³. Note that higher order post-Newtonian affects on the inspiral will be important in breaking the degeneracy between the individual masses of the objects and the chirp mass as well as deducing spins of the NS and BH.

We assume a 5-year observation with LISA, beginning at a GW frequency of 0.04 Hz and ending with a GW frequency of 0.44 Hz at the ISCO. This observation is then used to constrain the DM density at different radii from the central IMBH, corresponding to different times during the inspiral.

The radio signal is due to resonant axion-photon conversion occurring when the plasma frequency matches the axion mass, $\omega_p = m_a/2\pi$. The relevant interaction term in the Lagrangian is given by

$$\mathcal{L} = -\frac{1}{4} g_{a\gamma\gamma} a F^{\mu\nu} \tilde{F}_{\mu\nu} = -\frac{1}{4} g_{a\gamma\gamma} a \mathbf{E} \cdot \mathbf{B} \quad (3)$$

² The NS orbital velocity grows roughly as $r^{-1/2}$, so that the DF force scales roughly as $r^{-\alpha+1}$.

³ Note that we only consider low redshift systems, $z \ll 1$, therefore we ignore any difference between lab and system frame.

where a is the axion field, $g_{a\gamma\gamma}$ is the axion-photon coupling and $F^{\mu\nu}$ is the electromagnetic field strength tensor and $\tilde{F}_{\mu\nu}$ its dual. Following Ref. [38] we use the Goldreich-Julian model for the NS plasma [87]. Using the WKB and stationary phase approximations, the radiated power is given by,

$$\frac{d\mathcal{P}}{d\Omega} \sim 2 \times p_{a\gamma} \rho_{\text{DM}}(r_c) v_c r_c^2, \quad (4)$$

where r_c is the radius at which conversion happens, v_c is the DM velocity at the conversion radius, $\rho_{\text{DM}}(r_c)$ is the DM density at the conversion radius, and $p_{a\gamma}$ is the energy transfer function. The energy transfer function is given by,

$$p_{a\gamma} \sim \frac{g_{a\gamma\gamma}^2 B(r_c)^2 L_{\text{conv}}^2}{2v_c}, \quad (5)$$

where $B(r_c) \sim (r_{\text{NS}}/r_c)^3$ is the magnetic field strength at the conversion radius, and $L_{\text{conv}} = \sqrt{2\pi r_c v_c / 3m_a}$ is the length of the region over which conversion takes place. For the sake of simplicity, we consider the benchmark case of an aligned NS viewed at an angle of $\pi/2$ with respect to the NS rotation axis. In this case, we have $r_c = 5.8 \times 10^{-3} (1 \text{ eV}/m_a)^{2/3}$ km. A systematic study of the signal as a function of the angular configuration and time is in preparation [88].

We use Eddington's inversion formula to calculate the six-dimensional phase-space distribution function of the DM in the BH frame (see e.g. [89, 90]), assuming that the DM distribution is isotropic and spherically symmetric. This distribution $f(\mathcal{E})$ then depends on the relative energy $\mathcal{E} = \Psi(r) - \frac{1}{2}v^2$ and the relative gravitational potential $\Psi = \Phi_0 - \Phi$. For radii $r \lesssim 10^{-8}$ pc (the point at which the GW signal would become observable) the mass enclosed is dominated by the BH mass and we therefore neglect the contribution of the mini-spike to the relative potential: $\Psi = \Psi_{\text{BH}} = G_N M_{\text{BH}}/r$. In this case, we find $f(\mathcal{E}) \propto \mathcal{E}^{\alpha-3/2}$ (for $\mathcal{E} > 0$).

Nearby DM particles are accelerated under gravity as they infall toward the NS. Particles with initial velocity v reach a velocity $\sqrt{v^2 + 2\Psi_{\text{NS}}}$ at the conversion radius, where the NS potential is $\Psi_{\text{NS}} = G_N M_{\text{NS}}/r_c$. By applying Liouville's theorem [91], we find the DM density at the conversion radius to be,

$$\rho_{\text{DM}}(r_c) = \sqrt{\frac{2}{\pi}} \frac{\rho_{\text{sp}} r_{\text{sp}}^{\alpha}}{(G_N M_{\text{BH}})^{\alpha}} \frac{\alpha(\alpha-1)\Gamma(\alpha-1)}{\Gamma(\alpha-\frac{1}{2})} \times \int_{v_{\text{min}}}^{v_{\text{max}}} \left[\Psi_{\text{BH}} + \Psi_{\text{NS}} - \frac{v^2}{2} \right]^{\alpha-\frac{3}{2}} v^2 dv, \quad (6)$$

where $v_{\text{min}} = \sqrt{2\Psi_{\text{NS}}}$ and $v_{\text{max}} = \sqrt{2(\Psi_{\text{BH}} + \Psi_{\text{NS}})}$. We assume that the amplitude of the radiated power is dom-

inated by the peak of the velocity distribution⁴:

$$v_c^2 \sim \frac{2G_N M_{\text{BH}}}{r} \left[\alpha - \frac{1}{2} \right]^{-1} + \frac{2G_N M_{\text{NS}}}{r_c}. \quad (7)$$

Finally, the flux density of the radio signal is given by

$$S = \frac{1}{\mathcal{B} d^2} \frac{d\mathcal{P}}{d\Omega}, \quad (8)$$

where d is the distance of the system from us and \mathcal{B} is the bandwidth of the signal that is computed by calculating the 90% containment region of the DM velocity distribution far from the NS.

Results — We first show in Fig. 2 how the density of the DM halo can be reconstructed as a function of the radius from the IMBH. To calculate the error we take ten log-spaced radial bins (equivalently ten frequency bins) and integrate the noise weighted inner product between the associated lower and upper frequencies, f_l^i and f_u^i respectively. This allows us to calculate the Fisher information and thus the error on α :

$$\frac{\Delta\alpha}{\alpha} = \left[4 \text{Re} \left(\int_{f_l^i}^{f_u^i} \frac{\partial h}{\partial \ln \alpha} \frac{\partial h^*}{\partial \ln \alpha} df \right) \right]^{-\frac{1}{2}}, \quad (9)$$

where $S_n(f)$ is the LISA noise spectral density taken from Ref. [46] and h is the gravitational wave strain⁵. We neglect additional errors from the correlation between different parameters; Ref. [46] showed that for α they are relatively small. In addition, we assume that the masses and spins of the two objects can be measured in addition to the chirp mass, \mathcal{M}_c , when higher order effects are taken into account close to merger. This breaks the degeneracy between the normalisation and the slope of the density profile. Note that any additional errors from the determination of the individual masses and spins are not included here. A more detailed calculation of these errors is left to future work.

Figure 2 shows the 1σ uncertainty on the density reconstruction for our benchmark slope of $\alpha = 7/3$. At radii larger than $r \gtrsim 6 \times 10^{-9} \text{ pc}$, the DM density can be constrained to better than 10%, but as the separation of the binary decreases the uncertainty on the DM density increases. This is due to three effects; firstly, the gravitational interaction of the objects becomes greater closer to merger, leading GW emission (and not DF) to dominate the phase evolution of the waveform. Secondly, the number of cycles spent at a given radius is not evenly distributed, as can be seen by the upper y-axis of Fig. 2 which indicates the time to merger. Finally, the LISA sensitivity decreases at higher frequencies, weakening the

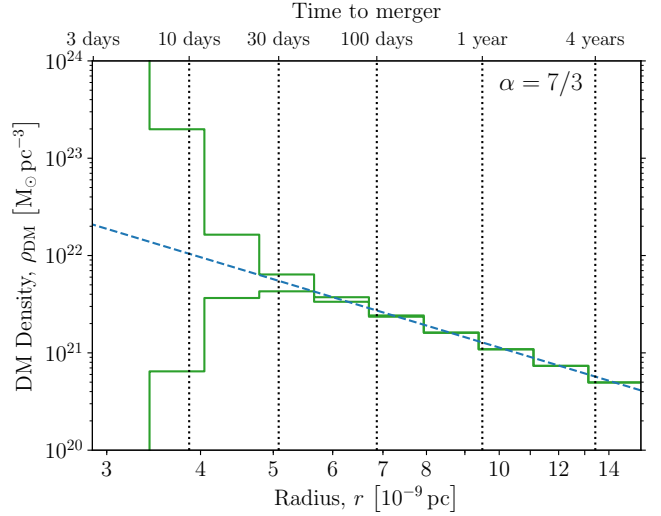


FIG. 2. **Error on the DM density from GW measurements of α .** Green bands show the 1σ uncertainties on the reconstructed DM density from analysing the GW waveform (for a system at $d = 10 \text{ Mpc}$ representing a signal-to-noise for LISA of ~ 92) over 10 bins in radius (measured from the position of the $10^4 M_\odot$ IMBH). The fiducial density profile with $\alpha = 7/3$ is shown as a blue dashed line. Along the top axis we also label the approximate time-to-merger as a function of radius in the vacuum case.

constraining power at small r . The phase evolution of the waveform is therefore very sensitive to the DM dynamical friction (and therefore the DM density) predominantly when the radial separation r is large. Such constraints on the density can then be fed directly into the EM signal calculation, predicting the expected radio emission.

In Fig. 3, we show the projected sensitivity curves of the future SKA telescope to the axion parameter space for two different distances d of the IMBH-DM-NS system and two different radii r during the inspiral. They have been obtained by considering the minimum detectable flux density which provides a signal-to-noise ratio (SNR) equal to one. In particular, for a radio telescope,

$$\text{SNR} = \frac{S}{\text{SEFD}} \sqrt{n_{\text{pol}} \mathcal{B} \Delta t_{\text{obs}}}, \quad (10)$$

where $n_{\text{pol}} = 2$ is the number of polarizations, Δt_{obs} is the observation time and $\text{SEFD} = 0.098$ is the SKA system-equivalent flux density [37, 92]. By inverting this relation, we obtain the minimum axion-photon coupling probed as a function of the axion mass. In particular, by neglecting the second term in the expression (7) for the velocity v_c , one can show that roughly $g_{a\gamma\gamma}^{\text{min}} \sim m_a^{-1/2}$. In all cases, we consider an observation time of 100 hours. This is roughly the time spent by the system from the closest orbit we consider ($r = 3 \times 10^{-9} \text{ pc}$) until the merger.

As can be seen in the plot, a crucial parameter is the distance of the IMBH-DM-NS system since the flux density depends on its inverse square. On the other hand, the

⁴ Note that we do not consider the boost to the NS frame since the NS orbital velocity is subdominant with respect to the DM peak velocity.

⁵ * indicates the complex conjugate.

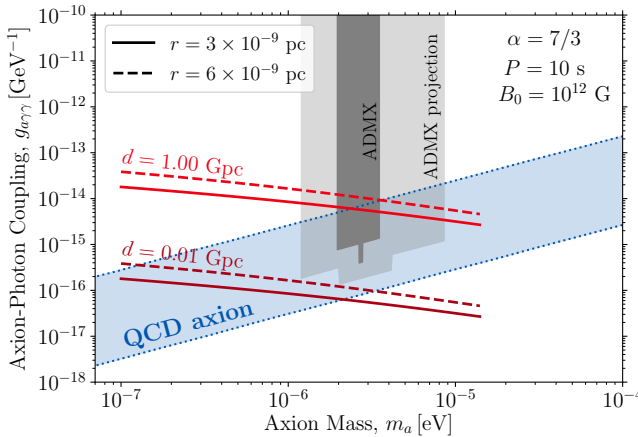


FIG. 3. Projected sensitivity to the axion-photon coupling from radio observations. Sensitivity curves of the SKA telescope (100 hours of observation) to the axion-photon coupling as a function of the axion mass for two different inspiral orbits, $r = 6 \times 10^{-9}$ pc (dashed) and $r = 3 \times 10^{-9}$ pc (solid), and two different IMBH-DM-NS system locations, $d = 0.01$ Gpc (dark red) and $d = 1.00$ Gpc (light red). Here, we assume $\alpha = 7/3$ for the slope of the DM spike. The predicted range of parameters for the QCD axion are represented by the blue band, while the vertical gray bands show the current and future ADMX limits [22, 23].

sensitivity curves do not strongly depend on the relative distance r between the BH and the NS. Radio observations taken when $r \sim 3 \times 10^{-9}$ pc (solid lines) yield sensitivities to $g_{a\gamma\gamma}$ which are roughly a factor of 2 greater than for $r \sim 6 \times 10^{-9}$ pc (dashed lines). In Fig. 3, we have fixed ρ_{DM} to the fiducial density profile. However, as we saw in Fig. 2, the DM density is likely to be more poorly constrained at smaller radii, making the radio sensitivity at large r substantially more robust (though not substantially weaker).

Discussion — With a sufficiently nearby detection of such a BH-NS system, it will be possible to probe the natural parameter space of the QCD axion. We find roughly a 0.05% probability of a detection closer than $d = 0.01$ Gpc over 10 years, using predicted LISA detection rates for such systems [75] (though these typically come with large uncertainties). Instead, out to $d = 1$ Gpc, we expect a few tens of detections per year. Here we have considered the observation of a single benchmark system, but detecting and studying a larger population of such

systems would allow us to strengthen the projections we present here.

A joint GW+EM detection would be a striking confirmation of axion dark matter. Though in some scenarios the dense DM spike would not be preserved [73, 74], GW observations can be used to confirm (or disfavor) the presence of a spike in a given system, as demonstrated in Fig. 2. The better estimation of the DM density at larger separations should reduce the uncertainties on the expected radio signal. Finally, we stress that one can take advantage of a greater observation time to probe smaller axion-photon couplings.

We have checked that the mini-spike should survive the merger itself; the work done by dynamical friction during the five year inspiral is only a few percent of the total gravitational binding energy of the halo. A more detailed study of feedback on the DM halo in different systems is in preparation [78]. We have also verified that the plasma remains bound to the NS; even down to the innermost orbit, the forces from the NS magnetosphere dominate over the gravitational force from the BH by many orders of magnitude. Thus, despite the violent environment, both signatures from GW and EM emission should be preserved.

Finally, we note that above around $m_a \sim 10^{-6}$ eV, these broadband sensitivities would be complementary to current and proposed axion haloscope experiments [22–27] (some of which are plotted in Fig. 3). These are sensitive to the density of DM local to Earth, which carries its own uncertainties [93]. Such uncertainties on the DM density can be mitigated in our scenario by combining information from GW and radio emission. Multi-messenger observations of Black Hole - Dark Matter - Neutron Star systems therefore have the potential to explore the natural parameter space of the QCD axion for masses between 10^{-7} eV and 10^{-5} eV.

ACKNOWLEDGMENTS

We thank David Nichols, Tanja Hinderer, Mikael Leroy, and Gianfranco Bertone for fruitful discussions. Finally, we thank the python scientific computing packages numpy [94] and scipy [95]. This research is funded by NWO through the VIDI research program “Probing the Genesis of Dark Matter” (680-47-532; TE, CW).

[1] G. Bertone, D. Hooper, and J. Silk, *Phys. Rept.* **405**, 279 (2005), arXiv:hep-ph/0404175 [hep-ph].
[2] G. Bertone and M. P. Tait, Tim, *Nature* **562**, 51 (2018), arXiv:1810.01668 [astro-ph.CO].
[3] L. D. Duffy and K. van Bibber, *New J. Phys.* **11**, 105008 (2009), arXiv:0904.3346 [hep-ph].
[4] T. MarrodÁn Undagoitia and L. Rauch, *J. Phys.* **G43**, 013001 (2016), arXiv:1509.08767 [physics.ins-det].
[5] J. M. Gaskins, *Contemp. Phys.* **57**, 496 (2016), arXiv:1604.00014 [astro-ph.HE].
[6] F. Kahlhoefer, *Int. J. Mod. Phys.* **A32**, 1730006 (2017), arXiv:1702.02430 [hep-ph].
[7] M. Dine, in *Flavor physics for the millennium. Proceedings, Theoretical Advanced Study Institute in elementary*

particle physics, *TASI 2000, Boulder, USA, June 4-30, 2000* (2000) pp. 349–369, arXiv:hep-ph/0011376 [hep-ph].

[8] R. D. Peccei and H. R. Quinn, *Phys. Rev. Lett.* **38**, 1440 (1977), [,328(1977)].

[9] R. D. Peccei and H. R. Quinn, *Phys. Rev.* **D16**, 1791 (1977).

[10] S. Weinberg, *Phys. Rev. Lett.* **40**, 223 (1978).

[11] F. Wilczek, *Phys. Rev. Lett.* **40**, 279 (1978).

[12] A. Arvanitaki, S. Dimopoulos, S. Dubovsky, N. Kaloper, and J. March-Russell, *Phys. Rev.* **D81**, 123530 (2010), arXiv:0905.4720 [hep-th].

[13] M. Dine, W. Fischler, and M. Srednicki, *Phys. Lett.* **104B**, 199 (1981).

[14] A. R. Zhitnitsky, Sov. J. Nucl. Phys. **31**, 260 (1980), [Yad. Fiz.31,497(1980)].

[15] J. E. Kim, *Phys. Rev. Lett.* **43**, 103 (1979).

[16] M. A. Shifman, A. I. Vainshtein, and V. I. Zakharov, *Nucl. Phys.* **B166**, 493 (1980).

[17] S. Hoof, F. Kahlhoefer, P. Scott, C. Weniger, and M. White, *JHEP* **03**, 191 (2019), arXiv:1810.07192 [hep-ph].

[18] D. J. E. Marsh, *Phys. Rept.* **643**, 1 (2016), arXiv:1510.07633 [astro-ph.CO].

[19] O. Wantz and E. P. S. Shellard, *Phys. Rev.* **D82**, 123508 (2010), arXiv:0910.1066 [astro-ph.CO].

[20] A. Salvio, A. Strumia, and W. Xue, *JCAP* **1401**, 011 (2014), arXiv:1310.6982 [hep-ph].

[21] M. Kawasaki, K. Saikawa, and T. Sekiguchi, *Phys. Rev.* **D91**, 065014 (2015), arXiv:1412.0789 [hep-ph].

[22] S. J. Asztalos *et al.* (ADMX), *Phys. Rev. Lett.* **104**, 041301 (2010), arXiv:0910.5914 [astro-ph.CO].

[23] N. Du *et al.* (ADMX), *Phys. Rev. Lett.* **120**, 151301 (2018), arXiv:1804.05750 [hep-ex].

[24] B. M. Brubaker *et al.*, *Phys. Rev. Lett.* **118**, 061302 (2017), arXiv:1610.02580 [astro-ph.CO].

[25] A. Caldwell, G. Dvali, B. Majorovits, A. Millar, G. Raffelt, J. Redondo, O. Reimann, F. Simon, and F. Steffen (MADMAX Working Group), *Phys. Rev. Lett.* **118**, 091801 (2017), arXiv:1611.05865 [physics.ins-det].

[26] L. Zhong *et al.* (HAYSTAC), *Phys. Rev.* **D97**, 092001 (2018), arXiv:1803.03690 [hep-ex].

[27] P. Brun *et al.* (MADMAX), *Eur. Phys. J.* **C79**, 186 (2019), arXiv:1901.07401 [physics.ins-det].

[28] M. Lawson, A. J. Millar, M. Pancaldi, E. Vitagliano, and F. Wilczek, (2019), arXiv:1904.11872 [hep-ph].

[29] Y. Kahn, B. R. Safdi, and J. Thaler, *Phys. Rev. Lett.* **117**, 141801 (2016), arXiv:1602.01086 [hep-ph].

[30] B. T. McAllister, G. Flower, E. N. Ivanov, M. Goryachev, J. Bourhill, and M. E. Tobar, *Phys. Dark Univ.* **18**, 67 (2017), arXiv:1706.00209 [physics.ins-det].

[31] T. M. Shokair *et al.*, *Int. J. Mod. Phys.* **A29**, 1443004 (2014), arXiv:1405.3685 [physics.ins-det].

[32] S. Al Kenany *et al.*, *Nucl. Instrum. Meth.* **A854**, 11 (2017), arXiv:1611.07123 [physics.ins-det].

[33] D. Alesini, D. Babusci, D. Di Gioacchino, C. Gatti, G. Lamanna, and C. Ligi, (2017), arXiv:1707.06010 [physics.ins-det].

[34] A. Caputo, C. P. Garay, and S. J. Witte, *Phys. Rev.* **D98**, 083024 (2018), [Erratum: *Phys. Rev.* D99,no.8,089901(2019)], arXiv:1805.08780 [astro-ph.CO].

[35] A. Caputo, M. Regis, M. Taoso, and S. J. Witte, *JCAP* **1903**, 027 (2019), arXiv:1811.08436 [hep-ph].

[36] I. G. Irastorza and J. Redondo, *Prog. Part. Nucl. Phys.* **102**, 89 (2018), arXiv:1801.08127 [hep-ph].

[37] B. R. Safdi, Z. Sun, and A. Y. Chen, (2018), arXiv:1811.01020 [astro-ph.CO].

[38] A. Hook, Y. Kahn, B. R. Safdi, and Z. Sun, *Phys. Rev. Lett.* **121**, 241102 (2018), arXiv:1804.03145 [hep-ph].

[39] F. P. Huang, K. Kadota, T. Sekiguchi, and H. Tashiro, *Phys. Rev.* **D97**, 123001 (2018), arXiv:1803.08230 [hep-ph].

[40] B. P. Abbott *et al.* (LIGO Scientific, Virgo), *Phys. Rev. Lett.* **116**, 061102 (2016), arXiv:1602.03837 [gr-qc].

[41] B. P. Abbott *et al.* (LIGO Scientific, Virgo), *Phys. Rev. Lett.* **119**, 161101 (2017), arXiv:1710.05832 [gr-qc].

[42] B. P. Abbott *et al.* (LIGO Scientific, Virgo, Fermi GBM, INTEGRAL, IceCube, AstroSat Cadmium Zinc Telluride Imager Team, IPN, Insight-Hxmt, ANTARES, Swift, AGILE Team, 1M2H Team, Dark Energy Camera GW-EM, DES, DLT40, GRAWITA, Fermi-LAT, ATCA, ASKAP, Las Cumbres Observatory Group, OzGrav, DWF (Deeper Wider Faster Program), AST3, CAASTRO, VINROUGE, MASTER, J-GEM, GROWTH, JAGWAR, CaltechNRAO, TTU-NRAO, NuSTAR, Pan-STARRS, MAXI Team, TZAC Consortium, KU, Nordic Optical Telescope, ePESSTO, GROND, Texas Tech University, SALT Group, TOROS, BOOTES, MWA, CALET, IKI-GW Follow-up, H.E.S.S., LOFAR, LWA, HAWC, Pierre Auger, ALMA, Euro VLBI Team, Pi of Sky, Chandra Team at McGill University, DFN, ATLAS Telescopes, High Time Resolution Universe Survey, RIMAS, RATIR, SKA South Africa/MeerKAT), *Astrophys. J.* **848**, L12 (2017), arXiv:1710.05833 [astro-ph.HE].

[43] D. Baumann, H. S. Chia, and R. A. Porto, *Phys. Rev.* **D99**, 044001 (2019), arXiv:1804.03208 [gr-qc].

[44] O. A. Hannuksela, K. W. K. Wong, R. Brito, E. Berti, and T. G. F. Li, *Nature Astron.* (2019), 10.1038/s41550-019-0712-4, arXiv:1804.09659 [astro-ph.HE].

[45] K. Eda, Y. Itoh, S. Kuroyanagi, and J. Silk, *Phys. Rev. Lett.* **110**, 221101 (2013), arXiv:1301.5971 [gr-qc].

[46] K. Eda, Y. Itoh, S. Kuroyanagi, and J. Silk, *Phys. Rev.* **D91**, 044045 (2015), arXiv:1408.3534 [gr-qc].

[47] C. F. B. Macedo, P. Pani, V. Cardoso, and L. C. B. Crispino, *Astrophys. J.* **774**, 48 (2013), arXiv:1302.2646 [gr-qc].

[48] E. Barausse, V. Cardoso, and P. Pani, *Phys. Rev.* **D89**, 104059 (2014), arXiv:1404.7149 [gr-qc].

[49] H. Audley *et al.* (LISA), (2017), arXiv:1702.00786 [astro-ph.IM].

[50] P. Bull *et al.*, (2018), arXiv:1810.02680 [astro-ph.CO].

[51] M. C. Miller and D. P. Hamilton, *Mon. Not. Roy. Astron. Soc.* **330**, 232 (2002), arXiv:astro-ph/0106188 [astro-ph].

[52] N. Webb, D. Cseh, E. Lenc, O. Godet, D. Barret, S. Corbel, S. Farrell, R. Fender, N. Gehrels, and I. Heywood, *Science* **337**, 554 (2012), arXiv:1311.6918 [astro-ph.HE].

[53] A. Ballone, M. Mapelli, and M. Pasquato, "Mon. Not. Roy. Astron. Soc." **480**, 4684 (2018), arXiv:1809.01664 [astro-ph.GA].

[54] S. Takekawa, T. Oka, Y. Iwata, S. Tsujimoto, and M. Nomura, "Astrophys. J." **871**, L1 (2019), arXiv:1812.10733 [astro-ph.GA].

[55] J.-H. Woo, H. Cho, E. Gallo, E. Hodges-Kluck, H. A. Le, J. Shin, D. Son, and J. C. Horst, arXiv e-prints , arXiv:1905.00145 (2019), arXiv:1905.00145 [astro-ph.GA].

[56] Y. Taniguchi, Y. Shioya, T. G. Tsuru, and S. Ikeuchi, *Publ. Astron. Soc. Jap.* **52**, 533 (2000), arXiv:astro-ph/0002389 [astro-ph].

[57] S. F. Portegies Zwart and S. L. W. McMillan, *Astrophys. J.* **576**, 899 (2002), arXiv:astro-ph/0201055 [astro-ph].

[58] S. F. Portegies Zwart, H. Baumgardt, P. Hut, J. Makino, and S. L. W. McMillan, *Nature* **428**, 724 (2004), arXiv:astro-ph/0402622 [astro-ph].

[59] M. C. Begelman, M. Volonteri, and M. J. Rees, *Mon. Not. Roy. Astron. Soc.* **370**, 289 (2006), arXiv:astro-ph/0602363 [astro-ph].

[60] B. Agarwal, S. Khochfar, J. L. Johnson, E. Neistein, C. Dalla Vecchia, and M. Livio, "Mon. Not. Roy. Astron. Soc." **425**, 2854 (2012), arXiv:1205.6464 [astro-ph.CO].

[61] B. J. Carr and M. J. Rees, *Mon. Not. Roy. Astron. Soc.* **206**, 801 (1984).

[62] R. Bean and J. Magueijo, *Phys. Rev. D* **66**, 063505 (2002), arXiv:astro-ph/0204486 [astro-ph].

[63] B. Carr, in *Symposium on Illuminating Dark Matter Kruen, Germany, May 13-19, 2018* (2019) arXiv:1901.07803 [astro-ph.CO].

[64] H.-S. Zhao and J. Silk, *Phys. Rev. Lett.* **95**, 011301 (2005), arXiv:astro-ph/0501625 [astro-ph].

[65] G. Bertone, A. R. Zentner, and J. Silk, *Phys. Rev. D* **72**, 103517 (2005), arXiv:astro-ph/0509565 [astro-ph].

[66] R. R. Islam, J. E. Taylor, and J. Silk, *Mon. Not. Roy. Astron. Soc.* **340**, 647 (2003), arXiv:astro-ph/0208189 [astro-ph].

[67] V. Rashkov and P. Madau, *Astrophys. J.* **780**, 187 (2014), arXiv:1303.3929 [astro-ph.CO].

[68] P. Gondolo and J. Silk, *Phys. Rev. Lett.* **83**, 1719 (1999), arXiv:astro-ph/9906391 [astro-ph].

[69] G. D. Quinlan, L. Hernquist, and S. Sigurdsson, *Astrophys. J.* **440**, 554 (1995), arXiv:astro-ph/9407005 [astro-ph].

[70] G. Bertone, G. Sigl, and J. Silk, *Mon. Not. Roy. Astron. Soc.* **337**, 98 (2002), arXiv:astro-ph/0203488 [astro-ph].

[71] G. Bertone, M. Fornasa, M. Taoso, and A. Zentner, *New J. Phys.* **11**, 105016 (2009), arXiv:0905.4736 [astro-ph.HE].

[72] J. F. Navarro, C. S. Frenk, and S. D. M. White, *Astrophys. J.* **462**, 563 (1996), arXiv:astro-ph/9508025 [astro-ph].

[73] P. Ullio, H. Zhao, and M. Kamionkowski, *Phys. Rev. D* **64**, 043504 (2001), arXiv:astro-ph/0101481 [astro-ph].

[74] D. Merritt, M. Milosavljevic, L. Verde, and R. Jimenez, *Phys. Rev. Lett.* **88**, 191301 (2002), arXiv:astro-ph/0201376 [astro-ph].

[75] G. Fragine, I. Ginsburg, and B. Kocsis, *Astrophys. J.* **856**, 92 (2018), arXiv:1711.00483 [astro-ph.GA].

[76] P. C. C. Freire, in *Neutron Stars and Pulsars: Challenges and Opportunities after 80 years*, IAU Symposium, Vol. 291, edited by J. van Leeuwen (2013) pp. 243–250, arXiv:1210.3984.

[77] I. Mandel, D. A. Brown, J. R. Gair, and M. C. Miller, *Astrophys. J.* **681**, 1431 (2008), arXiv:0705.0285 [astro-ph].

[78] D. A. Nichols, B. J. Kavanagh, G. Bertone, D. Gaggero, *et al.*, in preparation (2019).

[79] A. G. Lyne, R. N. Manchester, and N. D'Amico, "Astrophys. J. Lett." **460**, L41 (1996).

[80] J. D. Biggs, M. Bailes, A. G. Lyne, W. M. Goss, and A. S. Fruchter, "Mon. Not. Roy. Astron. Soc." **267**, 125 (1994).

[81] A. G. Lyne, J. D. Biggs, P. A. Harrison, and M. Bailes, "Nature" **361**, 47 (1993).

[82] N. Ivanova, C. O. Heinke, F. A. Rasio, K. Belczynski, and J. M. Fregeau, "Mon. Not. Roy. Astron. Soc." **386**, 553 (2008), arXiv:0706.4096.

[83] J. Boyles, D. R. Lorimer, P. J. Turk, R. Mnatsakanov, R. S. Lynch, S. M. Ransom, P. C. Freire, and K. Belczynski, "Astrophys. J." **742**, 51 (2011), arXiv:1108.4402 [astro-ph.SR].

[84] S. Chandrasekhar, *The Astrophysical Journal* **97**, 255 (1943).

[85] S. Chandrasekhar, *The Astrophysical Journal* **97**, 263 (1943).

[86] S. Chandrasekhar, *The Astrophysical Journal* **98**, 54 (1943).

[87] P. Goldreich and W. H. Julian, "Astrophys. J." **157**, 869 (1969).

[88] M. Leroy, C. Weniger, T. D. P. Edwards, and M. Chianese, in preparation (2019).

[89] J. Binney and S. Tremaine, *Galactic Dynamics: Second Edition*, by James Binney and Scott Tremaine. ISBN 978-0-691-13026-2 (HB). Published by Princeton University Press, Princeton, NJ USA, 2008. (Princeton University Press, 2008).

[90] R. Catena and P. Ullio, *JCAP* **1205**, 005 (2012), arXiv:1111.3556 [astro-ph.CO].

[91] J. Liouville, *J. Math. Pure. Appl.* **3**, 342 (1838).

[92] P. Dewdney, "SKA1 SYSTEM BASELINE DESIGN," https://www.skatelescope.org/wp-content/uploads/2012/07/SKA-TEL-SKO-DD-001-1_BaselineDesign1.pdf, accessed: 2019-05-21.

[93] J. I. Read, *J. Phys.* **G41**, 063101 (2014), arXiv:1404.1938 [astro-ph.GA].

[94] T. Oliphant, "NumPy: A guide to NumPy," USA: Trelgol Publishing (2006–), [Online; accessed 08/05/2019].

[95] E. Jones, T. Oliphant, P. Peterson, *et al.*, "SciPy: Open source scientific tools for Python," (2001–), [Online; accessed 08/05/2019].

[96] R. N. Manchester, G. B. Hobbs, A. Teoh, and M. Hobbs, *Astron. J.* **129**, 1993 (2005), arXiv:astro-ph/0412641 [astro-ph].

[97] C.-A. Faucher-Giguere and V. M. Kaspi, *Astrophys. J.* **643**, 332 (2006), arXiv:astro-ph/0512585 [astro-ph].

[98] S. B. Popov, J. A. Pons, J. A. Miralles, P. A. Boldin, and B. Posselt, *Mon. Not. Roy. Astron. Soc.* **401**, 2675 (2010), arXiv:0910.2190 [astro-ph.HE].

A Unique Multi-Messenger Signal of QCD Axion Dark Matter

Supplementary Material

Thomas D. P. Edwards, Marco Chianese, Bradley J. Kavanagh, Samaya M. Nissanke, and Christoph Weniger

This Supplementary Material is organized as follows: In App. I we discuss both the gravitational wave and radio signals dependence on the Dark Matter (DM) spike parameters. Appendix II discusses the velocity distribution of the DM, highlighting its limitations and how it can be addressed in future work. Finally, App. III discusses the dependence of the radio signal on the Neutron Star (NS) parameters. Here, we also speculate about the amplification of the radio signal if the neutron star had magnetic field strengths up to 10^{15} G or spin periods down to 0.1 s.

I. GRAVITATIONAL WAVES AND SPIKE DEPENDENCE

The phase difference between a vacuum inspiral and the one considered here is given by,

$$\Delta\Psi = \tilde{\Phi} - \Phi, \quad (\text{S1})$$

where $\Phi = -\frac{3}{4} (8\pi G M_c f/c^3)^{-5/3}$ is the Newtonian vacuum phase evolution and $\tilde{\Phi}$ is the phase evolution including dynamical friction, as given by Eq. (28c) of Ref. [46]. The phase evolution of the gravitational wave signal provides a fundamental insight into the dynamics of the binary system. As shown in Fig. S1, the presence of a DM spike (with $\alpha > 2.0$) produces a considerable phase shift when compared to the evolution of a vacuum inspiral. Again for $\alpha > 2.0$, the specific phase evolution of any particular system can therefore be used to constrain α to extremely high precision. For $\alpha < 2.0$, the phase difference becomes increasingly difficult to probe. Assuming the masses of the two objects can be independently measured to high precision, the constraint on α provides a direct constraint on the DM density local to the position of the NS [78]. We do not account for errors on the overall normalisation of the DM density profile directly. The normalisation can also be measured, though it is degenerate with M_{NS} and M_{BH} . To resolve the individual masses, higher order effects close to merger need to be accounted for. The errors associated with the individual mass determinations may dominate the error on the DM density normalisation at larger radii, but this is beyond the scope of the paper. We will address this in future work.

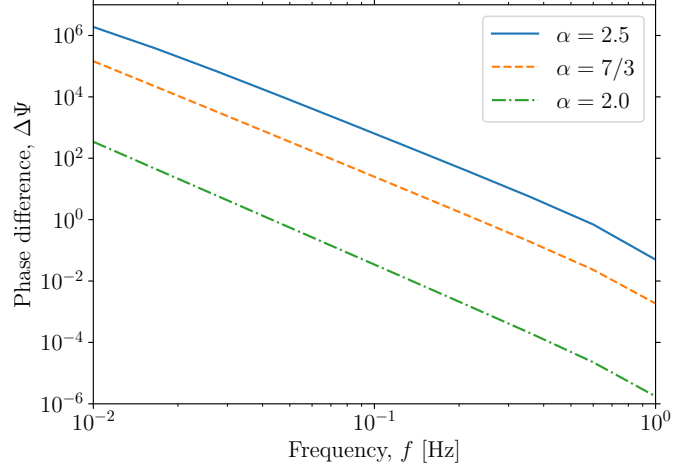


FIG. S1. **Phase difference between vacuum and DM spike inspiral.** We show the difference in the phase evolution of the IMBH-DM-NS system compared to a vacuum IMBH-NS inspiral for $\alpha = \{2.0, 7/3, 2.5\}$. As α is increased, the phase difference becomes larger. Similarly, the phase difference continues to be significant for higher frequencies when $\alpha > 7/3$. This persistent phase shift for large α is reflected as tighter constraints on the DM density, as seen in Fig. S2.

Figure S2 shows the constraint on the DM density from the GW signal, as described in the main text. The left and right panels show the constraint for $\alpha = 2.0$ and $\alpha = 2.5$, respectively. The error bars become larger for lower values of α ; this can easily be understood from Fig. S1. As the inspiral progresses, the GW frequency becomes larger (equivalently, the radius decreases). Similarly, the phase difference becomes ever smaller, gradually approaching the vacuum inspiral phase evolution and therefore providing no probe of the DM density. As α is increased, the large phase differences persist further into the inspiral, allowing one to probe the DM density closer to the IMBH.

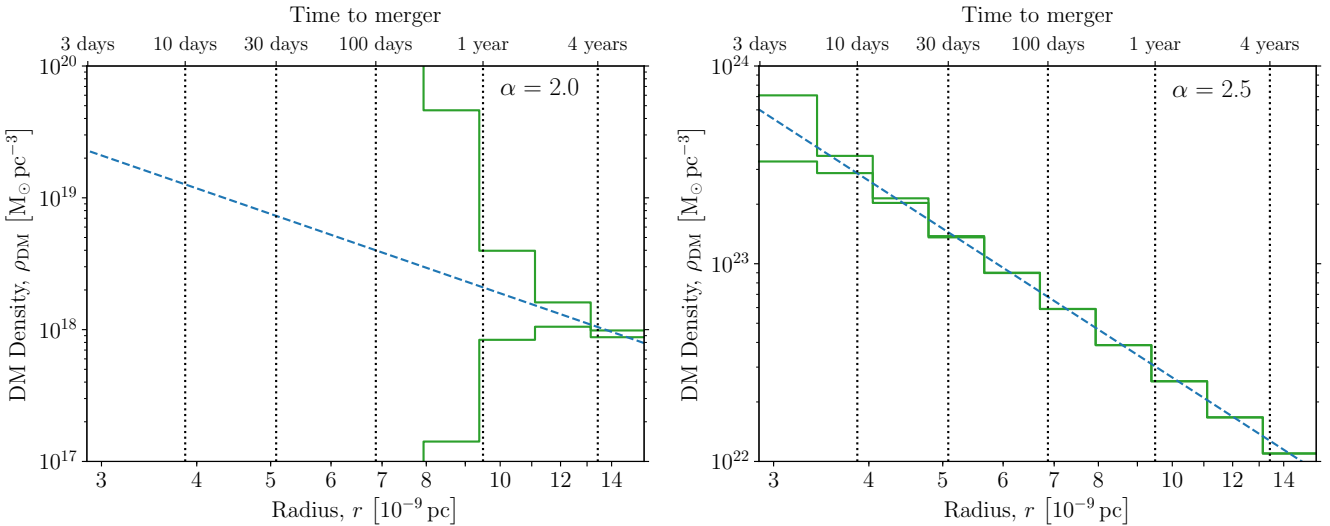


FIG. S2. **Error on the DM density from GW measurements of α .** Green bands show the 1σ uncertainties on the reconstructed DM density from analysing the GW waveform (for a system at $d = 10$ Mpc) over 10 bins in radius (measured from the position of the $10^4 M_\odot$ IMBH). The fiducial density profiles are shown as a blue dashed line with $\alpha = \{2.0, 7/3, 2.5\}$ on the left and right respectively. Along the top axis we also label the approximate time-to-merger as a function of radius in the vacuum case.

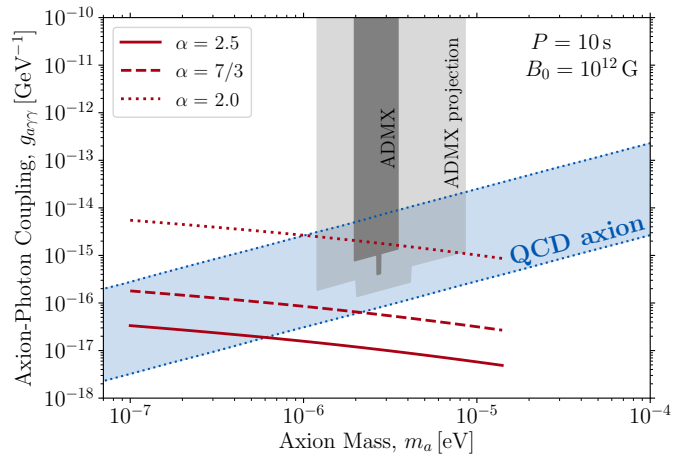


FIG. S3. **Projected sensitivity to the axion-photon coupling from radio observations.** Sensitivity curves of the SKA telescope (100 hours of observation) to the axion-photon coupling as a function of the axion mass for $\alpha = \{2.0, 7/3, 2.5\}$. Here, we assume a radial separation of $r = 3 \times 10^{-9}$ pc, $d = 0.01$ Gpc for the distance to the system, $B_0 = 10^{12}$ G for the NS magnetic field, and $P = 10$ s as the NS spin period. The predicted range of parameters for the QCD axion are represented by the blue band, while the vertical gray bands show the current and future ADMX limits [22, 23].

Finally, in Fig. S3 we present the radio sensitivity for $\alpha = \{2.0, 7/3, 2.5\}$. As expected, the varying density, as shown in Fig. S2, amplifies or decreases the density close the IMBH. For $\alpha = 2.0$, it is still possible to probe a small range of the QCD axion parameter space, although the constraint on the DM density becomes significantly worse (see left panel of Fig. S2). When $\alpha = 2.5$, the density can be constrained extremely well down to small radii. The density is also increased by an order of magnitude compared to the $\alpha = 7/3$ scenario, subsequently increasing the sensitivity by a similar amount.

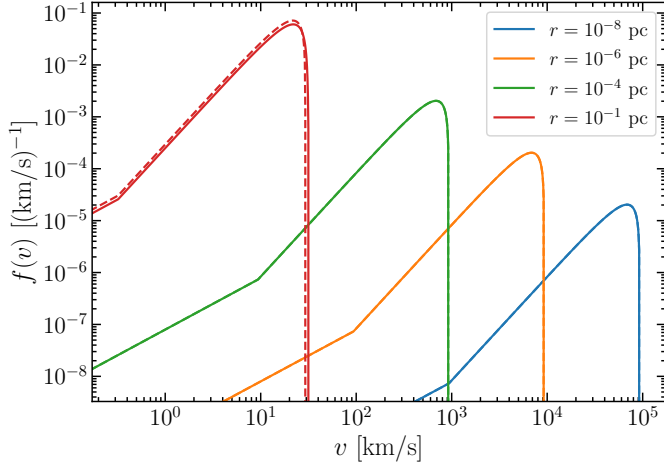


FIG. S4. **Dark Matter Speed distributions.** DM speed distribution derived from the Eddington Inversion formula, Eq. (S2), at different distances r from the central IMBH, $M_{\text{IMBH}} = 10^4 M_{\odot}$. Solid lines show the full calculation accounting for the potential due to the DM halo itself, while dashed lines show the approximate result, Eq. (S5), including on the potential due to the IMBH. Here, we assume $\alpha = 7/3$.

II. DARK MATTER VELOCITY DISTRIBUTION

We assume that the distribution of DM around the central black hole is spherically symmetric and that the velocity distribution of DM particles is isotropic. In this case, we can calculate the DM distribution function using Eddington's Inversion Formula:

$$f(\mathcal{E}) = \frac{1}{\sqrt{8\pi^2}} \int_0^{\mathcal{E}} \frac{d\Psi}{\sqrt{\mathcal{E} - \Psi}} \frac{d^2\rho}{d\Psi^2}. \quad (\text{S2})$$

Here, $\rho(r)$ is the density profile of the DM particles, while $\Psi(r)$ is the total gravitational potential, which in general includes a contribution from both the central mass and the mass enclosed in the DM halo. However, at small radii, the enclosed DM mass is small and we can typically neglect the contribution of the DM halo itself to the gravitational potential. We thus write $\Psi(r) = G_N M_{\text{BH}}/r$ and re-express the density in terms of the potential:

$$\rho(\Psi) = \rho_{\text{sp}} \left(\frac{r_{\text{sp}}}{G_N M_{\text{BH}}} \right)^\alpha \Psi^\alpha. \quad (\text{S3})$$

We therefore find:

$$\begin{aligned} f(\mathcal{E}) &= \frac{\alpha(\alpha-1)}{\sqrt{8\pi^2}} \rho_{\text{sp}} \left(\frac{r_{\text{sp}}}{G_N M_{\text{BH}}} \right)^\alpha \int_0^{\mathcal{E}} \Psi^{\alpha-2} \frac{d\Psi}{\sqrt{\mathcal{E} - \Psi}} \\ &= \frac{\alpha(\alpha-1)}{(2\pi)^{3/2}} \rho_{\text{sp}} \left(\frac{r_{\text{sp}}}{G_N M_{\text{BH}}} \right)^\alpha \frac{\Gamma(\alpha-1)}{\Gamma(\alpha-\frac{1}{2})} \mathcal{E}^{\alpha-3/2}. \end{aligned} \quad (\text{S4})$$

The DM speed distribution at a radius r is then given by

$$f(v|r) = 4\pi v^2 \frac{f(\Psi(r) - \frac{1}{2}v^2)}{\rho(r)} = \frac{4}{\sqrt{\pi}} \frac{\Gamma(\alpha+1)}{\Gamma(\alpha-\frac{1}{2})} \frac{v^2}{v_{\text{max}}^{2\alpha}} (v_{\text{max}}^2 - v^2)^{\alpha-3/2}. \quad (\text{S5})$$

Here, we have defined $v_{\text{max}} = v_{\text{max}}(r) = \sqrt{2\Psi(r)}$, and we set the speed distribution to zero for $v > v_{\text{max}}(r)$. With this definition, the speed distribution is normalised to one at any given radius:

$$\int_0^{v_{\text{max}}(r)} f(v|r) dv = 1. \quad (\text{S6})$$

In Fig. S4, we show the DM speed distribution at several radii r , assuming $\alpha = 7/3$ and $M_{\text{IMBH}} = 10^4 M_{\odot}$. Solid lines show the speed distribution derived from a full numerical calculation of $f(\mathcal{E})$ (using Eq. (S4) and including

self-consistently the potential due to the DM halo). Dashed lines show the approximate speed distribution given in Eq. (S5) (neglecting the potential of the DM halo itself). We see that in all cases of interest to us, $r \lesssim 10^{-8}$ pc, Eq. (S5) provides an excellent approximation to the full expression.

Finally, we note that as $r \rightarrow r_{\text{ISCO}}$, the maximum DM speed tends towards the speed of light. As we discuss in the main text, the dominant effect from dynamical friction typically occurs at larger radii, where the DM speeds are lower and the non-relativistic formalism should apply. However, at a radius $r = 3 \times 10^{-9}$ pc, the maximum DM speed is $v_{\text{max}} \approx 1.7 \times 10^5$ km/s $\approx 0.56 c$. Adding also the infall velocity toward the conversion radius, the DM particles are accelerated up to $\sim 0.8 c$. This suggests that towards the end of the inspiral, our non-relativistic formalism would over-estimate the speeds which can be reached by the DM particles. However, even at $r = 3 \times 10^{-9}$ pc, the DM speeds are still only mildly relativistic ($\gamma \sim 1.7$), suggesting that this should be a small effect. We leave a more detailed analysis – including relativistic effects, boosting in the NS rest-frame and anisotropy of the infalling DM flux – to future work.

III. NEUTRON STAR PARAMETERS

The NS parameters that regulate the amplitude of the radio signal (produced by the resonant axion-photon conversion) are the magnetic field strength at the NS poles B_0 and the spin period P . Together, they define the conversion radius given by

$$r_c \simeq 5.8 \times 10^{-3} \text{ km} \times |3 \cos \theta - 1|^{1/3} \left(\frac{r_{\text{NS}}}{10 \text{ km}} \right) \left[\frac{B_0}{10^{12} \text{ G}} \frac{10 \text{ s}}{P} \left(\frac{1 \text{ eV}}{m_a} \right)^2 \right]^{1/3}, \quad (\text{S7})$$

and, consequently, the magnetic field at r_c , which in the Goldreich-Julian model [87] takes the form

$$B(r_c) = \frac{B_0}{2} \left(\frac{r_{\text{NS}}}{r_c} \right)^3 (3 \cos^2 \theta + 1)^{1/2}, \quad (\text{S8})$$

where θ is the viewing angle that defines the direction of the Earth with respect to the NS axis. By plugging these expressions into Eqs. (4) and (5), we find the scaling with respect to B_0 and P to be

$$\frac{d\mathcal{P}}{d\Omega} \propto B_0 P \left(\frac{3 \cos^2 \theta + 1}{|3 \cos \theta - 1|} \right) [g_{a\gamma\gamma}^2 m_a \rho_{\text{DM}}(r_c) v_c]. \quad (\text{S9})$$

where the quantities in the squared parentheses are almost independent of the NS parameters. Hence, for a given axion mass, the larger the NS magnetic field and spin period, the larger the radiated power. Furthermore, the radiated power can be significantly larger for $\cos \theta = 1/3$; for other values of the viewing angle the radiated power is unaffected.

In Fig. S5 we report the projected sensitivity curves of SKA for three different values for the NS magnetic field strength (left panel) and three different values for the NS spin period (right panel), while fixing $r = 3 \times 10^{-9}$ pc, $d = 0.01$ Gpc, $\theta = \pi/2$ and $\alpha = 7/3$. As expected, the larger the magnetic field and the spin period, the smaller the axion-photon coupling that can be probed by SKA. Moreover, larger axion masses can be explored for larger magnetic fields or smaller spin periods. Equation (S7) shows that increasing B_0 , or decreasing P , causes axion-photon conversion to occur at a larger radius. The requirement $r_c \geq r_{\text{NS}} = 10$ km is then satisfied for a larger axion masses.

Finally, we note that the values for B_0 and P considered here cover almost all the possible properties of active NSs, according to the ATNF pulsar catalog [96]. On the other hand, old dead NSs are expected to have low magnetic fields and large spin periods, providing weaker sensitivities. However, their properties are quite uncertain and model-dependent [37, 97, 98].

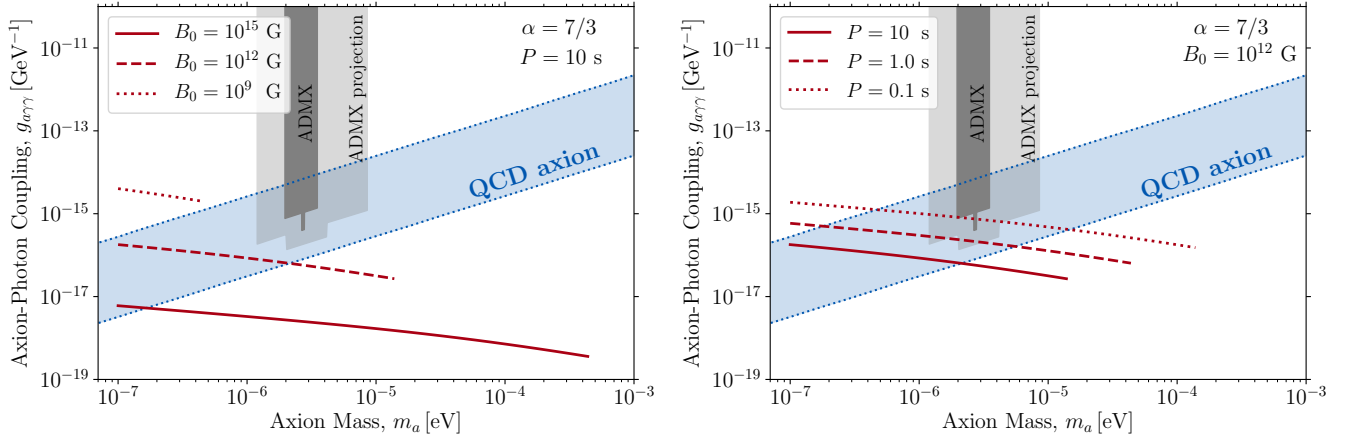


FIG. S5. **Projected sensitivity to the axion-photon coupling from radio observations.** Sensitivity curves of SKA telescope (100 hours of observation) to the axion-photon coupling as a function of the axion mass for three values of the NS magnetic field strength (left panel) and three values of the NS spin period (right panel). Here, we assume $\alpha = 7/3$ for the slope of the DM spike, $r = 3 \times 10^{-9}$ pc and $d = 0.01$ Gpc.